HEFAT2010
7th International Conference on Heat Transfer, Fluid Mechanics and Thermodynamics
19-21 July 2010
Antalya, Turkey

GRID REFINEMENT STUDIES OF FULLY DEVELOPED TURBULENT FLOW USING SECOND ORDER TURBULENCE MODELS

Afshar, M.
Department of Energy Engineering
Petroleum University of Technology
Tehran, Iran
E-mail: mafshar@put.ac.ir

ABSTRACT

Estimation of errors involved in the numerical prediction of fluid flow and heat transfer problems is an essential element in CFD. The errors involved in the numerical simulations can be categorized into two groups: modeling errors and numerical errors. For complex flows such as the turbulent flows, models which are simplified mathematical representation of the flow are prone to errors in realizing the flow behavior. Numerical errors are caused by the discretization of the governing equations and approximations of boundary conditions, non-convergence of iterative solution procedures, and round-off errors. It is crucial to minimize the numerical errors and evaluate the total errors precisely. The main objective of this paper is provide benchmark values for investigation of new turbulence models and to investigate the modeling and numerical errors encountered in the numerical simulation of the fully developed plane-channel flow using RSM with LRR and SSG pressure- strain second order turbulence models. Mesh refinement studies are reported with a fourth-order extrapolation scheme for flows with Reynolds numbers of 50000, 200000, and 500000. This study exclusively investigates the performance of staggered and colocated variable arrangements in providing stronger stress-strain rate couplings.
The near wall region is overpassed by implementation of the standard wall-function method. The results obtained are compared against the Laufer's experimental data and DS numerical results which enables evaluation of the accuracy of the second order turbulence models and grid arrangements as well as near-wall grid point location quantitatively for turbulent flows

INTRODUCTION

The crucial role of turbulence in most engineering flows necessitates the development and employment of methods which can be used in the simulation of such flows with acceptable accuracy. Since the mid of 1970's, second-order closure models have been developed for the calculations of turbulent flows. In these models, the Reynolds stress transport equation, where flow history and non-local effects are accounted for, are being solved for the calculation of turbulent stresses. These Reynolds Stress Models (RSM) have successfully overcome many deficiencies of the more popular k-ε turbulence models in capturing the important influences of curvature and body forces on the turbulent stresses [1]. Demuren and Sarkar [2] (denoted DS) made a systematic study of RSM's in the computation of plane-channel flows. They investigated three expressions for the turbulent diffusion terms and five models for the pressure-strain correlations. They concluded that the Mellor and Herring (1973) [3] denoted MH model for turbulent diffusion term produced the best agreement with experimental data; and the proposal of Launder, Reece, and Rodi [4] (denoted LRR) with wall-proximity treatment, and that of Speziale, Sarkar, and Gatski [5] (denoted SSG) pressure-strain models produced the best predictions of the Reynolds stresses.

Along with the advancements in the turbulence modelling, efforts have been made to develop numerical techniques for a more efficient implementation of these models. The stability of the solution is a vital parameter in CFD: in RSM turbulence modelling the stability can be enhanced by providing a strong coupling between the stresses and the associated primary 'driving' strains [1]. Two such measures are: 1) to stagger the stress locations relative to mean-velocity locations, and 2) to practice a special discretization method for the Reynolds stress gradients in momentum equations with collocated storage of all variables. Both of these methods have been widely used for the pressure-velocity couplings in fluid flow problems, for instance [6-7], and their merits and disadvantages for pressure-velocity couplings have been fully discussed [8]. These methods have also been implemented for the solution of turbulent flow problems with RSM's [9-10].

Estimation of errors involved in numerical prediction of fluid flows is another essential parameter in CFD. As Ferziger [11] suggested, the errors involved in the numerical simulation of fluid flows can be categorized into two groups: modelling errors and numerical errors. Models are usually a simplified mathematical representation of the physical problem of interest

and they are prone to errors in realizing the real problem: in particular for complex phenomenon such as turbulence. Numerical errors are caused by discretization of the governing equations and approximation of boundary conditions, non-convergence of iterative solution procedures, and round-off errors [5, 12]. It is crucial to delete or minimize the numerical errors, and in latter case to evaluate these errors accurately. It is expected that as the mesh is refined, the results would approach to the exact numerical solution of the modelled flow equations. Only, then, the modelling errors can be calculated by comparing the simulation results with experimental results. Furthermore, unless the numerical errors are smaller than the tolerable modelling errors, it would be impossible to assess the latter reliably [11].

The main objective of this paper is to provide benchmark values for the evaluation of turbulence models, and to investigate the modelling and numerical errors encountered in the numerical simulation of the fully developed turbulent plane-channel flow problem, using different models and numerical techniques. This problem has been investigated by many researchers. In a review of duct flow measurements by Klein [13] different available experimental data are evaluated. The Laufer's experimental results [14] was used by Demuren and Sarkar [2] to validate their numerical results.

This problem is solved in a one-dimensional Cartesian coordinate system. The turbulence is modelled using RSM with LRR and SSG pressure-strain models. Mesh-refinement studies are reported with a fourth-order accurate extrapolation scheme for flows of Reynolds number 50000, 200000, and 500000.

This study exclusively investigates the performance of staggered and collocated variable arrangements in providing stronger stress-strain-rate couplings.

In this study, the near wall region is overpassed by implementation of the standard wall-function method. To investigate the effect of the near-wall grid point location, the tests have been done at three nominal y^+ values of 30, 60, and 120. The results obtained in this study, for the flow with Re = 200000, are compared with the Laufer's experimental and DS numerical results.

GOVERNING EQUATIONS

The Reynolds-averaged mean-flow equations for incompressible turbulent low of a Newtonian Fluid can be written in Cartesian tensor notation as:

Continuity

$$\frac{\partial \overline{u}_i}{\partial x_i} = 0 \qquad (1)$$

Momentum

$$\rho\frac{\partial \overline{u}_i}{\partial t} + \rho\overline{u}_k\frac{\partial \overline{u}_i}{\partial x_k} = -\frac{\partial \overline{p}}{\partial x_k} + \frac{\partial}{\partial x_k}\left[-\rho\overline{u_i'u_k'} + \mu\left(\frac{\partial \overline{u}_i}{\partial x_k} + \frac{\partial \overline{u}_k}{\partial x_i}\right)\right] \qquad (2)$$

In this equation, ū and u' are the mean and fluctuating velocities, respectively, ρ is the density, $\overline{p}$ is the mean pressure, and μ is the viscosity. To solve these equations, the Reynolds stresses $\rho\overline{u_i'u_k'}$ should be calculated as a *priory*.

Reynolds Stress Equations

The Reynolds stress transport equation is derived from the momentum equation as in the following equation:

$$\overline{u_i' N(u_j) + u_j' N(u_i)} = 0.$$

The exact form of the Reynolds stress transport equation is:

$$\rho\frac{\partial \overline{u_i'u_j'}}{\partial t} + \rho\overline{u}_k\frac{\partial \overline{u_i'u_j'}}{\partial x_k} = -\left(\overline{u_i'u_k'}\frac{\partial \overline{u}_j}{\partial x_k} + \overline{u_j'u_k'}\frac{\partial \overline{u}_i}{\partial x_k}\right) - \frac{\partial}{\partial x_k}\left(\overline{u_i'u_j'u_k'} + \frac{\overline{pu_j'}}{\rho}\delta_{ik} + \frac{\overline{pu_i'}}{\rho}\delta_{jk} - \nu\frac{\partial \overline{u_i'u_j'}}{\partial x_k}\right) + \overline{\frac{p}{\rho}\left(\frac{\partial u_i'}{\partial x_j} + \frac{\partial u_j'}{\partial x_i}\right)} - 2\nu\frac{\partial \overline{u_i'}}{\partial x_k}\frac{\partial \overline{u_j'}}{\partial x_k} \qquad (3)$$

This equation can be cast in the following compact form;

$$\frac{D\overline{u_i'u_j'}}{Dx_k} = P_{ij} + d_{ij} + \Phi_{ij} - \varepsilon_{ij} \qquad (4)$$

LHS term is the material derivative of Reynolds stresses; the RHS terms are the *production*, the *diffusion*, the *pressure strain*, and the *dissipation* of the Reynolds stresses, respectively. The production term can be retained exactly and it does not need any modelling, but the other three terms on the RHS of eq. 4 should be modelled with suitable correlations. Regarding the DS results, in this paper the following models have been used,

Turbulent Diffusion Term,

MH model:

$$-\left(\overline{u_i'u_j'u_k'}\right) = c_s\frac{k^2}{\varepsilon}\left[\left(\overline{u_i'u_j'}\right)_{,k} + \left(\overline{u_i'u_k'}\right)_{,j} + \left(\overline{u_j'u_k'}\right)_{,i}\right]$$

where, k and ε are the turbulent kinetic energy and its dissipation rate, respectively, and $c_s = 0.22/3$.

Pressure Strain Term

LRR model with wall-proximity treatment

$$\overline{\frac{p}{\rho}\left(\frac{\partial u_i'}{\partial x_j} + \frac{\partial u_j'}{\partial x_i}\right)} = \phi_{(1)ij} + \phi_{(2)ij} + \phi_{(w1)ij} + \phi_{(w2)ij}$$

where

$$\phi_{(1)ij} = c_1\frac{\varepsilon}{k}\left(\overline{u_i'u_j'} - \frac{2}{3}\delta_{ij}k\right) \qquad \phi_{(2)ij} = c_2\left(P_{ij} - \frac{2}{3}\delta_{ij}P\right)$$

$$\phi_{(w1)ij} = c_{w1}\frac{\varepsilon}{k}\left(\overline{u_k'u_m'}n_kn_m\delta_{ij} - \frac{3}{2}\overline{u_k'u_i'}n_kn_j - \frac{3}{2}\overline{u_k'u_j'}n_kn_i\right)f$$

$$\phi_{(w2)ij} = c_{w2}\left(\phi_{(2)km}n_kn_m\delta_{ij} - \frac{3}{2}\phi_{(2)ik}n_kn_j - \frac{3}{2}\phi_{(2)jk}n_kn_i\right)f$$

P is the trace of P_{ij} tensor, n is the unit normal vector outward to the wall, and $f = k^{3/2}/(2.5\varepsilon d)$ is the wall reflection term (d is the distance to the wall). $c_1 = 1.8$, $c_2 = 0.6$, $c_{w1} = 0.5$, and $c_{w2} = 0.3$ in these expressions.

The values of coefficients are the values proposed by Craft et al. [15], these are different to the values which are proposed in the original LRR model [4].

SSG model:

$$\overline{\frac{p}{\rho}\left(\frac{\partial u_i'}{\partial x_j} + \frac{\partial u_j'}{\partial x_i}\right)} = -\left(c_1\varepsilon + c_1^*P\right)b_{ij} + c_2\varepsilon\left(b_{ik}b_{kj} - \frac{1}{3}b_{mn}b_{mn}\delta_{ij}\right) + \left(c_3 - c_3^*\left(b_{mn}b_{nm}\right)^{1/2}\right)k\bar{S}_{ij} + c_4k\left(b_{ik}\bar{S}_{jk} + b_{jk}\bar{S}_{ik} - \frac{2}{3}b_{mn}\bar{S}_{mn}\delta_{ij}\right) + c_5k\left(b_{ik}\bar{W}_{jk} + b_{jk}\bar{W}_{ik}\right)$$

Where $\bar{S}_{ij} = \frac{1}{2}\left(\frac{\partial \bar{u}_i}{\partial x_j} + \frac{\partial \bar{u}_j}{\partial x_i}\right)$ and $\bar{W}_{ij} = \frac{1}{2}\left(\frac{\partial \bar{u}_i}{\partial x_j} + \frac{\partial \bar{u}_j}{\partial x_i}\right)$ are the symmetric and anti-symmetric parts of strain-rate tensor, respectively, and

$$b_{ij} = \left(\frac{\overline{u_i' u_j'}}{2k} - \frac{1}{3}\delta_{ij} k \right)$$

is the anisotropy tensor. $c_1 = 3.4$, $c_1^* = 1.8$, $c_2 = 4.2$, $c_3 = 0.8$, $c_3^* = 1.3$, $c_4 = 1.25$ and $c_5 = 0.4$ in this expression.

Dissipation Term

Kolmogorov model:

$$2\nu \overline{\frac{\partial u_i'}{\partial x_k} \frac{\partial u_j'}{\partial x_k}} = \frac{2}{3}\delta_{ij}\varepsilon$$

To close these set of equations, the turbulence energy dissipation rate equation is adopted from the work of Hanjalic and Launder (1972):

$$\frac{\partial \varepsilon}{\partial t} + \bar{u}_k \frac{\partial \varepsilon}{\partial x_k} = \frac{\partial}{\partial x_k}\left[\left(\nu + c_\varepsilon \frac{k}{\varepsilon} \overline{u_k' u_l'} \right) \frac{\partial \varepsilon}{\partial x_l} \right] - c_{\varepsilon 1} \frac{\varepsilon \overline{u_i' u_k'}}{k} \frac{\partial \bar{u}_i}{\partial x_k} - c_{\varepsilon 2} \frac{\varepsilon^2}{k} \quad (5)$$

where, $c_{\varepsilon 1} = 1.44$ and $c_{\varepsilon 2} = 1.83$.

These equations are simplified for the fully developed flow in a channel as follows;

The momentum equation in the axial direction:

$$-\frac{\partial \bar{p}}{\partial x} + \frac{\partial}{\partial y}\left[-\rho \overline{u'v'} + \mu \left(\frac{\partial \bar{u}}{\partial y} \right) \right] = 0 \quad (6)$$

regarding the Reynolds stress equations, the LHS terms are zero and the RHS terms are as shown in table 1.

The ε equation simplifies to:

$$\frac{\partial}{\partial y}\left[\left(\nu + c_\varepsilon \frac{k}{\varepsilon} \overline{u'^2} \right) \frac{\partial \varepsilon}{\partial y} \right] - c_{\varepsilon 1} \frac{\varepsilon \overline{u'v'}}{k} \frac{\partial \bar{u}}{\partial y} - c_{\varepsilon 2} \frac{\varepsilon^2}{k} = 0 \quad (7)$$

In general, the governing equations for this problem can be cast in the following diffusion-type, steady, one-dimensional form:

$$\nabla.(\varsigma \nabla \phi) + S = 0 \quad (8)$$

Where, φ_j represents the transported scalar of interest; that is: ū, turbulent stresses, or ε; S involves all terms except the diffusion term, and ς is the diffusion coefficient.

NUMERICAL PROCEDURES

As was mentioned earlier, the Finite Volume Method (FVM) of Patankar and Spalding [16] has been implemented for the numerical simulation of fully developed turbulent plane-channel flow. This is a conduction-type, steady, one-dimensional problems; there are only the diffusion and the source terms in governing equations of this problem (eq. 8). The procedure outlined in [17] is used to discretize and assemble the discretized equations of dependent variables of interest.

The final form of discretized equations can be cast in the following general form

$$aP_j \phi_j = aE_j \phi_{j+1} + aW_j \phi_{j-1} + b_j \quad (9)$$

Discretization of $-\nabla.(\rho \overline{u'v'})$ term in ū equation (eq. 6), however, should be examined more carefully. If all the dependent variables are stored on the grid points, and the discretized form of the axial momentum equation (eq. 6) being constructed without any special treatment of stress-strain-rate coupling -- the discretized form of the $-\nabla.(\rho \overline{u'v'})$ term will take the following form for uniform grids.

$$\rho \overline{u'v'}_w - \rho \overline{u'v'}_e = \frac{\rho \overline{u'v'}_W - \rho \overline{u'v'}_P}{2} - \frac{\rho \overline{u'v'}_P - \rho \overline{u'v'}_E}{2} = \frac{\rho \overline{u'v'}_W - \rho \overline{u'v'}_E}{2}$$

As for pressure-velocity coupling in fluid flow problems two methods have been proposed; namely, staggering the

Table 1: RSM terms in fully developed plane channel flow

$\overline{u_i'u_k'}$	P_{ij}	d_{ij}	ε_{ij}	$\phi_{ij}(LRR)$
$\overline{u'^2}$	$-2\overline{u'v'}\frac{\partial \bar{u}}{\partial y}$	$\frac{\partial}{\partial y}\left[\left(\nu + c_s\frac{k^2}{\varepsilon}\right)\frac{\partial(\overline{u'^2})}{\partial y}\right]$	$\frac{2}{3}\varepsilon$	$-c_1\frac{\varepsilon}{k}\left(\overline{u'^2}-\frac{2}{3}k\right)+\frac{4}{3}c_2\overline{u'v'}\frac{\partial \bar{u}}{\partial y}$ $+\left(c_{w1}\frac{\varepsilon}{k}\overline{u'^2}-\frac{2}{3}c_2c_{w2}\overline{u'v'}\frac{\partial \bar{u}}{\partial y}\right)f$
$\overline{u'^2}$	0	$\frac{\partial}{\partial y}\left[\left(\nu + 3c_s\frac{k^2}{\varepsilon}\right)\frac{\partial(\overline{u'^2})}{\partial y}\right]$	$\frac{2}{3}\varepsilon$	$-c_1\frac{\varepsilon}{k}\left(\overline{u'^2}-\frac{2}{3}k\right)-\frac{2}{3}c_2\overline{u'v'}\frac{\partial \bar{u}}{\partial y}$ $+\left(-2c_{w1}\frac{\varepsilon}{k}\overline{u'^2}+\frac{4}{3}c_2c_{w2}\overline{u'v'}\frac{\partial \bar{u}}{\partial y}\right)f$
$\overline{w'^2}$	0	$\frac{\partial}{\partial y}\left[\left(\nu + c_s\frac{k^2}{\varepsilon}\right)\frac{\partial(\overline{w'^2})}{\partial y}\right]$	$\frac{2}{3}\varepsilon$	$-c_1\frac{\varepsilon}{k}\left(\overline{w'^2}-\frac{2}{3}k\right)-\frac{2}{3}c_2\overline{u'v'}\frac{\partial \bar{u}}{\partial y}$ $+\left(2c_{w1}\frac{\varepsilon}{k}\overline{u'^2}-\frac{2}{3}c_2c_{w2}\overline{u'v'}\frac{\partial \bar{u}}{\partial y}\right)f$
$\overline{u'v'}$	$\overline{u'^2}\frac{\partial \bar{u}}{\partial y}$	$\frac{\partial}{\partial y}\left[\left(\nu + 2c_s\frac{k^2}{\varepsilon}\right)\frac{\partial(\overline{u'v'})}{\partial y}\right]$	0	$-c_1\frac{\varepsilon}{k}\overline{u'v'}+\frac{2}{3}c_2\overline{u'^2}\frac{\partial \bar{u}}{\partial y}$ $+\left(-\frac{3}{2}c_{w1}\frac{\varepsilon}{k}\overline{u'v'}-\frac{3}{2}c_2c_{w2}\overline{u'^2}\frac{\partial \bar{u}}{\partial y}\right)f$
$\overline{u_i'u_k'}$	$\phi_{ij}(SSG)$			
$\overline{u'^2}$	$\frac{-\left(c_1\varepsilon - c_1^*\overline{u'v'}\frac{\partial \bar{u}}{\partial y}\right)}{2k}\overline{u'^2}+\frac{c_2\varepsilon}{3}\left[2\left(\frac{\overline{u'^2}}{2k}-\frac{1}{3}\right)^2-\left(\frac{\overline{u'^2}}{2k}-\frac{1}{3}\right)^2\right.$ $\left.-\left(\frac{\overline{w'^2}}{2k}-\frac{1}{3}\right)^2+\left(\frac{\overline{u'v'}}{2k}\right)^2\right]-\left(\frac{c_1^*}{3}-\frac{c_4}{6}-\frac{c_5}{2}\right)\overline{u'v'}\frac{\partial \bar{u}}{\partial y}+\frac{c_1\varepsilon}{3}$			
$\overline{u'^2}$	$\frac{-\left(c_1\varepsilon - c_1^*\overline{u'v'}\frac{\partial \bar{u}}{\partial y}\right)}{2k}\overline{u'^2}+\frac{c_2\varepsilon}{3}\left[-\left(\frac{\overline{u'^2}}{2k}-\frac{1}{3}\right)^2+2\left(\frac{\overline{u'^2}}{2k}-\frac{1}{3}\right)^2\right.$ $\left.-\left(\frac{\overline{w'^2}}{2k}-\frac{1}{3}\right)^2+\left(\frac{\overline{u'v'}}{2k}\right)^2\right]-\left(\frac{c_1^*}{3}-\frac{c_4}{6}-\frac{c_5}{2}\right)\overline{u'v'}\frac{\partial \bar{u}}{\partial y}+\frac{c_1\varepsilon}{3}$			
$\overline{w'^2}$	$\frac{-\left(c_1\varepsilon - c_1^*\overline{u'v'}\frac{\partial \bar{u}}{\partial y}\right)}{2k}\overline{w'^2}+\frac{c_2\varepsilon}{3}\left[-\left(\frac{\overline{u'^2}}{2k}-\frac{1}{3}\right)^2-\left(\frac{\overline{u'^2}}{2k}-\frac{1}{3}\right)^2\right.$ $\left.+2\left(\frac{\overline{w'^2}}{2k}-\frac{1}{3}\right)^2-2\left(\frac{\overline{u'v'}}{2k}\right)^2\right]-\left(\frac{c_1^*}{3}-\frac{c_3}{3}\right)\overline{u'v'}\frac{\partial \bar{u}}{\partial y}+\frac{c_1\varepsilon}{3}$			
$\overline{u'v'}$	$\frac{-\left(c_1\varepsilon - c_1^*\overline{u'v'}\frac{\partial \bar{u}}{\partial y}\right)}{2k}\overline{u'v'}+\frac{c_2\varepsilon}{2k}\left(\frac{\overline{u'^2}+\overline{v'^2}}{2k}-\frac{2}{3}\right)\overline{u'v'}$			

Table 1: RSM terms in fully developed plane channel flow

turbulent shear stresses to CV faces, or using a special treatment of stress-strain-rate couplings in a colocated approach. In staggered variable arrangement, the location of turbulent shear stress terms $\overline{u'v'}$ in channel flow are staggered to the main grid points and are located at the control volume faces. For this variable arrangement, the discretized form of $-\nabla.(\rho \overline{u'v'})$ term will be:

$$\rho\overline{u'v'}_w - \rho\overline{u'v'}_e = \rho\overline{u'v'}_P - \rho\overline{u'v'}_W$$

Therefore, the difference in turbulent shear stresses on the control volume faces is appearing in axial velocity equation. This approach will detect any oscillatory $\overline{u'v'}$ field and the stress-strain-rate coupling is preserved fully.

In the colocated approach the $-\nabla.(\rho\overline{u'v'})$ term in the momentum equation is replaced by an expression which is derived from a special treatment of turbulent shear stress discretized equations.

The discretized $\overline{u'v'}$ equations can be written as follows:

$$a_{P_j}\overline{u'v'}_j = a_{E_j}\overline{u'v'}_{j+1} + a_{W_j}\overline{u'v'}_{j-1} + b'_j - \left(1 - c2 + \frac{3}{2}c'_2 f_y\right)\overline{v}'^2_j \frac{\partial\bar{u}}{\partial y}\Delta V_j \qquad (10)$$

b'_j is the constant term without the contribution of terms including $\frac{\partial\bar{u}_j}{\partial y}$ and ΔV_j is the CV volume. This equation can be written as:

$$\overline{u'v'}_j = \hat{\overline{u'v'}}_j - d\overline{u'v'}_j \frac{\partial\bar{u}_j}{\partial y} \qquad (11)$$

Where

$$\hat{\overline{u'v'}}_j = \frac{a_{E_j}\overline{u'v'}_{E_j} + a_{W_j}\overline{u'v'}_{W_j} + b'_2}{a_{P_j}}, d\overline{u'v'}_j = \frac{\Delta V_j}{a_{P_j}}\left(1 - c2 + \frac{3}{2}c'_2 f_y\right)\overline{v}'^2_j$$

The value of $\overline{u'v'}$ at interfaces is calculated by the following special treatment of strain-rate terms $\frac{\partial\bar{u}_j}{\partial y}$. The value of $\overline{u'v'}$ at the east interface is obtained by a linear interpolation of $\hat{\overline{u'v'}}$ and $d\overline{u'v'}$ at nodes j and j+1, and with the linear interpolation of velocity between these two nodes.

$$\overline{u'v'}_e = \left[\frac{\hat{\overline{u'v'}}_j + \hat{\overline{u'v'}}_{j+1}}{2}\right] - \left[\frac{d\overline{u'v'}_j + d\overline{u'v'}_{j+1}}{2}\right]\left(\frac{\bar{u}_{j+1} - \bar{u}_j}{(\delta y)_e}\right) \qquad (12)$$

or:

$$\overline{u'v'}_e = \hat{\overline{u'v'}}_e - d\overline{u'v'}_e\left(\frac{\bar{u}_{j+1} - \bar{u}_j}{(\delta y)_e}\right) \qquad (13)$$

where:

$$\hat{\overline{u'v'}}_e = \left[\frac{\hat{\overline{u'v'}}_j + \hat{\overline{u'v'}}_{j+1}}{2}\right] \qquad d\overline{u'v'}_e = \left[\frac{d\overline{u'v'}_j + d\overline{u'v'}_{j+1}}{2}\right]$$

Integrate the ū equation over the control volume j;

$$\left[\mu\frac{\partial\bar{u}_j}{\partial y}\right]_w^e - \frac{\partial\bar{p}_j}{\partial x}\Delta V - \left[\rho\overline{u'v'}_j\right]_w^e = 0$$

Substitute for interfacial $\overline{u'v'}_j$ values from eq. 13, and rearrange;

$$\left[\left(\mu + \rho d\overline{u'v'}_j\right)\frac{\partial\bar{u}_j}{\partial y}\right]_e - \left[\left(\mu + \rho d\overline{u'v'}_j\right)\frac{\partial\bar{u}_j}{\partial y}\right]_w - \frac{\partial\bar{p}_j}{\partial x}\Delta V - \left(\rho\hat{\overline{u'v'}}_j\right)_e + \left(\rho\hat{\overline{u'v'}}_j\right)_w = 0 \qquad (14)$$

If this equation is compared with the generalized form for the diffusion-type, steady, one-dimensional problems,

$$\varsigma = \left(\mu + \rho d\overline{u'v'}_j\right) \qquad and \qquad S = -\frac{\partial\bar{p}_j}{\partial x}\Delta V - \left(\rho\hat{\overline{u'v'}}_j\right)_e + \left(\rho\hat{\overline{u'v'}}_j\right)_w$$

for the $\bar{u}$ equations.

Extrapolation Procedure

The proposed extrapolation procedure is based on the work of Richardson [18]. The key idea is to consider the final, converged, numerical result as itself being an analytic function of the grid size. The results of these grid tests are fitted to some appropriate analytic function, which is then used to obtain, or extrapolate grid-independent result [19].

. If the relative change in φ values of all dependent variables of interest in the two trails $\left|\frac{\Phi_2 - \Phi_1}{\Phi_1}\right|$ is less than 10^{-4}, then, these φ_2 values are the grid-independent values of the dependent variables; otherwise this procedure is repeated with a finer grid size until the specified criterion is satisfied.

BOUNDARY CONDITIONS

The equations derived in the previous section are not applicable for the flow close to the wall. A wall-function approach is used to overpass this area: it's based on the assumption of local-equilibrium turbulence and validity of the logarithmic wall of law in this region. Consistent with this are the following relations:

$$k = \frac{u_\tau^2}{\sqrt{c_\mu}} \qquad \varepsilon = \frac{u_\tau^3}{ky} \qquad \frac{\partial\bar{u}}{\partial y}x = \frac{u_\tau}{ky} \qquad P_k = \varepsilon \qquad (15)$$

where κ is the Von Karman constant equal to 0.41 and $u_\tau = \sqrt{\tau_w/\rho}$ is the friction velocity. The values of Reynolds stresses in the log-law region are calculated by substituting the above equations in Reynolds-stress transport eqs. table 1;

LRR Model:

$$\overline{u}'^2 = 1.098k, \quad \overline{v}'^2 = 0.247k, \quad \overline{w}'^2 = 0.655k, \quad \overline{u'v'} = -0.255k. \qquad (16)$$

SSG Model:

$$\overline{u}'^2 = 1.098k, \quad \overline{v}'^2 = 0.247k, \quad \overline{w}'^2 = 0.655k, \quad \overline{u'v'} = -0.255k. \qquad (17)$$

At the channel centre line, the gradient of all variables are set to zero, except turbulent shear stress terms which take a value of zero.

Numerical Details

In this work, the grid-independent extrapolated values have been obtained for bulk mean velocity $\bar{u}_b$, friction factor f, and $\bar{u}$, k, and ε values at the channel centre for these cases:

- Simple, colocated, and staggered variable arrangements using RSM with LRR pressure-strain model,
- Colocated and staggered variable arrangements using RSM with SSG pressure-strain model,

for the following Reynolds numbers and y^+ values;

- Re = 200000, and nominal y^+ values of 30, 60, and 120.
- Re = 50000 and 500000 with nominal y^+ values of 30.

These tests provide enough material to investigate the effects of turbulence modelling, variable arrangements, location of the near wall grid point on the grid-independent results for fully-developed turbulent flow in a channel at different Reynolds numbers. The Demuren-Sarkar results are obtained at Reynolds number of 200000 (based on the channel hydraulics diameter and bulk mean velocity) which coincides with the highest Reynolds number of Laufer's experimental results. Results produced in this work at Re = 200000 are compared with Laufer's experimental and DS numerical results.

RESULTS

Grid-Independent Results

Grid-independent results are presented in tables 2 to 7 and figs. 1 and 2. To display the trend of the converged results, the values of f, $\bar{u}_c$, $\bar{u}_b$, $k_c/\bar{u}_b^2$, $\varepsilon_c H/\bar{u}_b^3$, ($c$ stands for the channel center) for converged solutions of fully-developed plane-channel flow with different variables arrangements and turbulence modeling for a nominated $y^+ = 30$ at $Re = 200000$ are presented in table 2. These values are tabulated for the final five grid sizes ($n = n_1$ to n_5) with the converged results which have been used to obtain the final extrapolated grid-independent results, Φ_1 and Φ_2. As it can be seen, in each case, the converged results are monotonically advancing toward the grid-independent results; hence, the proposed procedure can be used to calculate the extrapolated grid-independent values of the flow parameters [19].

These values are tabulated for $\bar{u}_c/\bar{u}_b$, $k_c/\bar{u}_b^2$ and $\varepsilon_c H/\bar{u}_b^3$ at three nominated y^+ values for the flow at Re = 200000, table 3. These values, as reported here, are with seven significant figures, but they have been calculated with nine significant figures accuracy.

Table 2: Converged results for Re = 200000, $y^+ = 30$

MODEL	n	$10^2 f$	$\bar{u}_c/\bar{u}_b$	$10^3 k_c/\bar{u}_b^2$	$10^5 \epsilon_c H/\bar{u}_b^3$
RSM-LRR (Simple)	601	1.448916	1.096236	2.550259	7.429512
	701	1.448844	1.096233	2.550151	7.428992
	801	1.448798	1.096231	2.550082	7.428654
	901	1.448766	1.096230	2.550033	7.428421
	1001	1.448743	1.096229	2.549999	7.428254
	Φ_1	1.448720	1.096224	2.549853	7.427546
	Φ_2	1.448770	1.096226	2.549853	7.427557
RSM-LRR (Colocated)	401	1.449834	1.096270	2.551774	7.436411
	451	1.449520	1.096258	2.551262	7.434065
	501	1.449312	1.096251	2.550922	7.432506
	601	1.449064	1.096241	2.550517	7.430649
	701	1.448930	1.096236	2.550301	7.429651
	Φ_1	1.448670	1.096232	2.549880	7.427847
	Φ_2	1.448700	1.096226	2.550085	7.428261
RSM-LRR (Staggered)	601	1.433978	1.095832	2.523183	7.313592
	701	1.436369	1.095895	2.527545	7.332137
	801	1.438102	1.095941	2.530704	7.345591
	901	1.439413	1.095975	2.533092	7.355773
	1001	1.440439	1.096003	2.534958	7.363735
	Φ_1	1.448620	1.096225	2.549820	7.427403
	Φ_2	1.448650	1.096224	2.549826	7.427443
RSM-SSG (Colocated)	501	1.781343	1.093953	2.001345	6.818693
	601	1.781474	1.093951	2.001537	6.819523
	701	1.781531	1.093949	2.001628	6.819894
	801	1.781555	1.093947	2.001672	6.820062
	901	1.781564	1.093946	2.001695	6.820136
	Φ_1	1.781430	1.093934	2.001555	6.819256
	Φ_2	1.781390	1.093939	2.001621	6.819594
RSM-SSG (Staggered)	301	1.845901	1.095348	2.075831	7.197474
	351	1.835682	1.095122	2.064087	7.137117
	401	1.828183	1.094957	2.055465	7.092934
	451	1.822462	1.094831	2.048886	7.059291
	501	1.817964	1.094732	2.043710	7.032871
	Φ_1	1.781370	1.093935	2.001521	6.819208
	Φ_2	1.781500	1.093937	2.001637	6.819767

As expected, among the other variables, the ε_c extrapolated values satisfied the extrapolation criterion $\left(\left|\frac{\Phi_2-\Phi_1}{\Phi_1}\right| < 10^{-4}\right)$ after all the other variables. The ε governing equation is more source dominated than $\bar{u}$, and k governing equations -- regarding the assumption that the values of the source terms components Sc and Sp prevail over the corresponding control volumes (first order approximation); while the diffusion terms are interpolated via a second-order scheme -- it would require finer grids results to compensate for its poorer converged results accuracy (closer to first order).

Table-3: Extrapolated values for Re = 200000

MODEL	y^+	$10^2 f$	$\bar{u}_c/\bar{u}_b$	$10^3 k_c/\bar{u}_b^2$	$10^5 \epsilon_c H/\bar{u}_b^3$
RSM-LRR (Simple)	30	1.448770	1.096226	2.549853	7.427557
	60	1.408760	1.095575	2.474582	7.116900
	120	1.403890	1.095879	2.456422	7.066679
RSM-LRR (Colocated)	30	1.448700	1.096226	2.550085	7.428261
	60	1.408800	1.095576	2.474525	7.116752
	120	1.403870	1.095879	2.456452	7.066707
RSM-LRR (Staggered)	30	1.448650	1.096224	2.549826	7.427443
	60	1.408750	1.095575	2.474550	7.116808
	120	1.403870	1.095880	2.456381	7.066485
RSM-SSG (Colocated)	30	1.781390	1.093939	2.001621	6.819594
	60	1.781710	1.093005	2.004343	6.823640
	120	1.855620	1.092089	2.096274	7.261308
RSM-SSG (Staggered)	30	1.781500	1.093937	2.001637	6.819767
	60	1.781930	1.093008	2.004594	6.824902
	120	1.855660	1.092085	2.096668	7.262697

Considering the relative error in the results obtained with a coarser grid (n = 101) to grid independent values, table 4, it exposes the importance of selecting the most relevant variable (or parameter) when the converged numerical-results are studied for the grid-refinement effects. As it is evident from table 4, while these relative errors are of order of less than 1% for $\bar{u}_c$ values, talking of a converged result which will not change considerably with grid-refinement is fallacy; since the largest relative errors are encountered in the ε_c values (up to 20 %), this is the most relevant variable for monitoring grid-independency of the results.

The grid-independent results for three nominated y^+ values are shown in table 3 and the relative errors for the results obtained with a grid size n = 101 are also shown for the smallest and largest nominated y^+ values in table 4. It is obvious that the y^+ values have an effect on the final grid-independent values through their influence on the boundary-conditions information transmission to the interior of the domain. Also, regarding the fact that the larger the y^+ value, the near-wall grid point will be furtherer from the wall, and, hence, the changes in variables are more gradual; therefore, the iterative solution should converge faster. In addition, the extrapolated grid-independent values are obtained with converged solutions on the smaller number of grid points for higher y^+ values. This implies that the relative errors in the converged solution on the same grid-size be smaller for the solutions with a nominated $y^+ = 120$ than the corresponding solution with a nominated $y^+ = 30$ as shown in the table 4.

The variable arrangement, as expected, does not have any impact on the final grid-independent results, table 3; however, it has a pronounce effect on the number of iterations to achieve a converged solution to this problem on a particular grid number, table 5, and the corresponding relative errors to grid-independent values.

In general, for the RSM's, the co-located variable arrangement converges to a solution at a higher number of iterations and the staggered variable arrangement at a lower number of iterations. The staggered variable arrangement could not produce any converged results for smaller number of grid

points (they produce converged solution if the solution by another approach was introduced as the guess values for the start of the program).

Table 4: Relative errors in results with a grid size of 101 for Re = 200000

MODEL	y^+	f	$\bar{u}_c/\bar{u}_b$	$10^3 k_c/\bar{u}_b^2$	$10^5 \epsilon_c H/\bar{u}_b^3$
RSM-LRR (Simple)	30	0.53	0.03	0.45	0.76
	120	0.11	0.00	0.15	0.19
RSM-LRR (Colocated)	30	2.10	0.09	2.01	3.12
	120	0.52	0.02	0.47	0.75
RSM-LRR (Staggered)	30	8.48	0.28	8.90	12.65
	120	7.12	0.18	7.53	10.61
RSM-SSG (Colocated)	30	0.21	0.02	0.37	2.73
	120	0.86	0.02	0.92	1.31
RSM-SSG (Staggered)	30	12.44	0.45	12.70	19.47
	120	8.17	0.22	8.56	12.75

Table 5: iteration numbers to achieve converged solution at Re = 200000

MODEL	y^+	51	101	151	201	251
RSM-LRR (Original)	30	2312	4012	4303	7795	2089
	120	1073	1932	969	1299	2503
RSM-LRR (Colocated)	30	2276	2126	4266	7696	2214
	120	2335	4342	4573	7843	2007
RSM-LRR (Staggered)	30	-	1185	1539	1920	2335
	120	-	1305	1742	2216	2723
RSM-SSG (Colocated)	30	1719	2408	3463	5856	9462
	120	1528	3360	7896	6695	10436
RSM-SSG* (Staggered)	30	-	-	2045	2303	2582
	120	-	-	2469	2923	3438

Figs. 1 and 2 show the relative errors of the converged solutions to grid-independent values of ε_c on five grid-sizes (51, 101, 151, 201, and 201) for two nominated y^+ values, 30 and 120. The relative error is changing from one turbulence model to the other model, and is dependent on the variable arrangement; nevertheless, in all cases, increasing the grid numbers decreases the relative error. The staggered variable arrangement results encounter the highest relative error values: this could be attributed to the location of the near-wall turbulent shear-stress term which is on the face of the second control-volume for other variables. As it was shown earlier, the location of near-wall points have a relatively considerable effect on the results; hence, in staggered variable arrangement, as the mesh is refined and the location of near-wall turbulent shear stress term changes and gets closer to the wall, the change in results are more than in other variable arrangements, and more grid points are needed to acquire the same relative accuracy (to grid-independent values) as the corresponding solutions with other variable arrangements. Colocated variable arrangement results are much closer to their corresponding grid-independent values on the coarser grids -- in particular with SSG model -- than other variable arrangements.

The performance of different turbulence models is not the same for different variable-arrangements. As shown in figs. 1 and 2, the SSG model with colocated variable arrangement results encounter the lowest relative error levels, and this model with staggered grid arrangement, also, produced the highest relative error levels among all the approaches. The LRR model with simple variable arrangement, the LRR with colocated variable-arrangements, and the LRR with staggered variable arrangement produced converged results with relative errors from lower to higher levels, respectively, are between these two extremes.

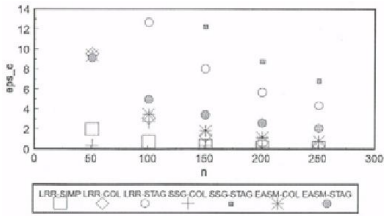

Figure 1: Relative errors to the grid-independent results, grid sizes 51-251, Re = 200000, y^+ = 30

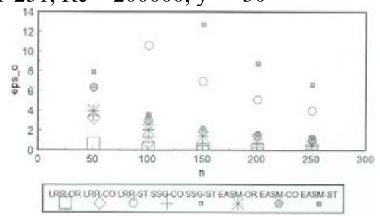

Figure 2: Relative errors to the grid-independent results, grid sizes 51-251, Re = 200000, y^+ = 120

Flow Profiles

The nondimensional velocity and turbulent kinetic energy ($\bar{u}/\bar{u}_b$ and k/u_τ^2) and the anisotropy tensor b_{11}, b_{22}, b_{33}, and b_{12} profiles along the channel width are shown in figs. 3 and 4. These are the same parameters which were also being used by Demuren and Sarkar [2]; hence, this makes it possible to compare the results obtained in this work -- in addition to the Laufer's experimental results [14] -- with the corresponding results in their work. The results shown in these figs. are obtained on a 251 uniformly spaced grids and a nominated y^+ = 30 value -- the corresponding relative errors to grid-independent values are shown in fig. 1 (maximum 7%). Since, basically, the results obtained for each turbulence model by different variable arrangements coincides exactly for this grid size; hence, only, the results are presented with indication of the turbulence model used.

The velocity profiles, fig. 3, show a perfect agreement with DS numerical and Laufer's experimental results for all the turbulent models. The turbulent kinetic energy profiles are shown in fig. 3; agreement among results is good except for the LRR model. The results produced by this model are neither in agreement with the DS results obtained with this model.

The reasons are two-folds:

1- the values of coefficients used in LRR pressure-strain model as implemented in this work are taken from a work by Launder and his co-workers [15], while the DS results are obtained by using the values presented in the original LRR paper [4]. It should be noted that in the original LRR paper, Launder et al. compared the turbulent intensity distributions with the experimental results of Comte-Bellot [20], and not with the Laufer's experimental results.

2- the less important reason is in the differences in the near-wall values of turbulent stresses used in this work and the DS work. In this work, these values are obtained by inserting

the relations 15 in the Reynolds stresses governing equations which results in the near-wall values presented in the eq. 16. This approach is also used by Lien and Leschziner [21] to fix the near-wall values of turbulent stresses. But, Demuren and Sarkar used the same near-wall values for all the models that they tested which is not necessarily the best method to fix these values.

The agreement between results produced in this work by SSG pressure-strain model are in good agreement with the Laufer's experimental results. The anisotropy tensor profiles, b_{11}, b_{22}, b_{33} and b_{12} are shown in fig. 4. The profiles obtained in this work with the SSG pressure-strain model are in full agreement with the corresponding results of Demuren and Sarkar. The results obtained with LRR pressure-strain model do not match with either experimental or numerical reference results, except for b_{11} profile which is in good agreement to Laufer's experimental results close to wall, but overestimates it in the channel center.

These results can be summarized as follows:

1. The results obtained from the SSG pressure-strain model are in full agreement with the corresponding DS numerical results, and show the same behavior against the Laufer's experimental results.
2. The results obtained with the LRR pressure-strain model does match neither with the corresponding DS numerical results, nor with the Laufer's experimental results. These are because of implementation of most recent and relevant approaches implemented in this work in comparison to the older corresponding proposals.

Reynolds Number Effects

To investigate the behavior of different turbulence models for flows with lower and higher Reynolds numbers, the problem was also solved for flows of two Reynolds numbers 50000 and 500000. These solution were obtained on staggered variable arrangement for a nominated $y^+ = 30$ which as shown earlier produced the highest relative error among the other configurations.

The extrapolated grid-independent values and the corresponding relative errors encountered in the solutions on a 101 grid size are shown in table 6. As expected, these error are higher for flows at RE = 500000 and lower for flows at RE = 50000 in comparison to the corresponding relative errors for flows at Re = 200000. As Reynolds number increases, the rate of change of flow parameters along the channel width increases, and, therefore, finer grids are needed to achieve the results with similar accuracies.

Table 6: Extrapolated values relative errors for Re = 50000 and 500000 at $y^+ = 30$ with staggered variable arrangement

Re	MODEL	$10^2 f$	$\bar{u}_c/\bar{u}_b$	$10^3 k_c/\bar{u}_b^2$	$10^5 \epsilon_c H/\bar{u}_b^3$
Re= 50000	RSM-LRR	2.002200	1.116611	3.448638	11.85169
	Error %	0.50	0.01	0.55	0.74
	RSM-SSG	2.484680	1.110909	2.760036	11.13435
	Error %	5.57	0.18	5.92	8.73
Re= 500000	RSM-LRR	1.220580	1.087212	2.158412	5.765924
	Error %	21.26	0.72	21.99	30.49
	RSM-SSG	1.497990	1.085620	1.689428	5.270872
	Error %	21.53	0.76	21.73	34.20

Similarly, the converged results to be used for obtaining extrapolated grid-independent should be obtained on finer grids as the Reynolds number increases.

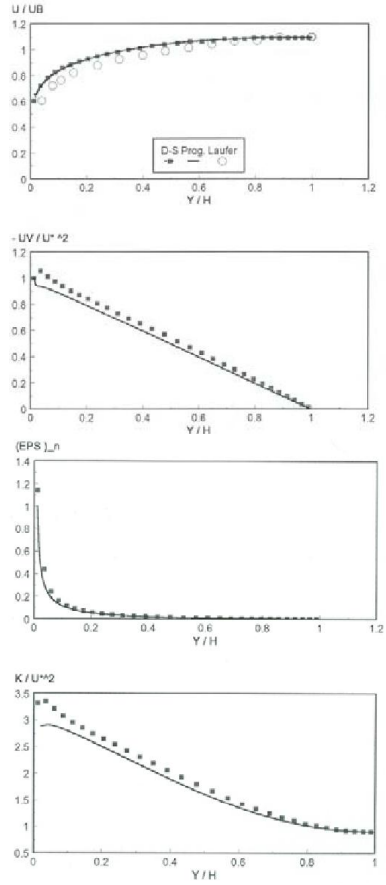

Figure 3: Comparison of results with DS's numerical and Laufer's experimental results, Re = 200000,y^+= 30, n = 251

CONCLUSIONS

In this paper benchmark values for investigation of new turbulence models are presented.. The modeling and numerical errors encountered in the numerical simulation of the fully developed plane-channel flow using RSM with LRR and SSG pressure- strain second order turbulence models are investigated.. Mesh refinement studies are reported with a fourth-order extrapolation scheme for flows with Reynolds numbers of 50000, 200000, and 500000. This study exclusively investigated the performance of staggered and colocated variable arrangements in providing stronger stress-strain rate couplings.

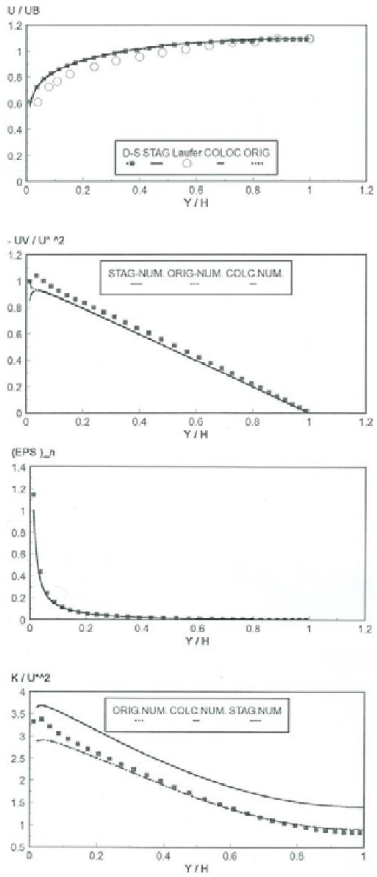

Figure 4: Comparison of results with DS's numerical and Laufer's experimental results, Re = 200000, $y^+ = 30$, n = 251.

REFERENCES

[1] Leschziner,M.A., Introduction to the Modelling of Turbulence, Von Karman Institute for Fluid Dynamics, *Lecture Series 1987-06*, 1987.

[2] Demuren,A.O. - Sarkar,S., Perspective: Systematic Study of Reynolds Stress Closure Models in the Computations of Plane Channel Flow, *ASME J. of Fluid Engg.*, Vol. 115, pp. 5-12, 1993.

[3] Mellor, G.L., Herring,H.J., A Survay of Mean Turbulent Field Closure, *AIAA Journal*, Vol. 11, pp. 590-599, 1973.

[4] Launder,B.E. - Reece,J., Rodi,W., Progress in the Development of A Reynolds-Stress Turbulence Closure, *J. Fluid Mechanics*, Vol. 68, Part 3, pp. 537-566, 1975.

[5] Speziale,C.G., Sarkar,S., Gatski,T.B., Modelling the Pressure-Strain Correlation of Turbulence: An Invarient Dynamical Systems Approach, *J. Fluid Mechanics*, Vol. 227, pp. 245-272, 1991.

[6] Harlow, F.H., Welch, J.E., Numerical Calculation of Time-Dependent Viscous Incompressible Flow of Fluid with Free Surface, *Phys. of Fluids*, Vol. 8, p. 2182, 1965.

[7] Peric, M., A Finite Volume Method for Prediction of Three Dimensional Fluid Flow in Complex Ducts, *Ph.D thesis submitted to the University of London,* London, UK, 1985.

[8] Peric, M., Kessler, R., Scheuerer, G., Comparison of Finite-Volume Numerical Methods with Staggered and Collocated Grids, *Computers and Fluids*, Vol. 16, No. 4, pp. 389-403, 1988.

[9] Hogg,S., Leschziner,M.A., Computing of Highlt Swirling Flow with A Reynolds Stress Turbulent Model, *AIAA Journal*, Vol. 27, No. 1, pp. 57-63, 1989.

[10] Obi,S., Peric,M., Scheuerer,G., Second-Moment Calculation Procedure for Turbulent Flows with Colocated Variable Arrangement, *AIAA Journal*, Vol. 29, No. 4, pp. 585-590, 1991.

[11] Ferziger, J.H., Estimation and Reduction of Numerical Error, *Proc. of the symp. on Qualification of Uncertainty in Computational Fluid Dynamics*, FED-Vol. 158, pp. 1-8, 1993.

[12] Roache,P.J., A Method for Uniform Reporting of Grid Refinement Studies, *ASME J. of Fluid Engg.*, Vol. 116, pp. 405-413, 1994.

[13] Klein, A., Review: Turbulent Developing Pipe Flow, *ASME J. of Fluid Engg.*, Vol. 103, pp. 4023-429, 1981.

[14] Laufer,J., Investigation of Turbulent Flow in a Two-Dimensional Channel, *N.A.C.A. REP*, No. 1053, 1951.

[15] Craft,T.J., Graham,L.J.W., Launder,B.E., Impinging Jet Studies for Turbulence Model Assessment, II. An Approximation of the Performance of Four Turbulence Models, Int. *J. Heat Mass Transfer*, Vol. 36, No. 10, pp. 2685-2697, 1993.

[16] Patankar, S.V., Spalding. D.B., A Calculation Procedure for Heat, Mass, and Momentum Transfer in Three-Dimensional Parabolic Flows, *Int. J. of Heat Mass Transfer*, Vol. 15, pp. 1787-1806, 1972.

[17] Patankar, S.V. *Numerical Heat Transfer and Fluid Flow*, Hemisphere Publishing Co., 1980.

[18] Richardson,L.F., The Approximate Arithmatic Solution by Finite Differences of Physical Problems Involving Differential Equations with an Application to the Stresses in a Masonry Dam, *Trans. Roy. Soc. London*, *Series A*, Vol. 210, pp. 307-357, 1910.

[19] Sebben,S., Baliga,B.R., A Benchmark Numerical Solution Involving Steady, Spatially-Periodic, Fully-Developed Laminar Flow and Heat Transfer, 1996.

[20] Comte-Bellot, G, Ecoulement: Turbulent Entre deux Parois Paralleles, *Publ. Sci. Tech. Ministere de l'air*, No. 419, 1965.

[21] Lien,F.S., Leschziner,M.A., Second-Moment Modelling of Reciculating Flow in A Non-Orthogonal Collocated Finite-Volume Algorithm, *Proc. 8th Symp. Turb. Shear Flows*, pp. 205-222, 1992.

NOMENCLATURE

k	Turbulent kinetic energy
ε	Dissipation of the Reynolds stresses
$\bar{u}$	Mean velocity
u'	Fluctuating velocity
$\rho\overline{u_i'u_k'}$	Reynolds stresses
$\bar{p}$	Mean pressure
P_{ij}	Production

Special characters

f	Friction factor
ς	Diffusion coefficient

Subscripts

j	Node number
i	Node number
e	East
w	West